Tortuosity in anode-supported proton conductive solid oxide fuel cell found from current flow rates and dusty-gas model

Authors: C.-L. Tsai and V. Hugo Schmidt

C.-L. Tsai and V.H. Schmidt, "Tortuosity in anode-supported proton conductive solid oxide fuel cell found from current flow rates and dusty-gas model," Journal of Power Sources 196, 692-699 (2011), doi: 10.1016/j.jpowsour.2010.08.005

Tortuosity in anode-supported proton conductive solid oxide fuel cell found from current flow rates and dusty-gas model

Chih-Long Tsai*, V. Hugo Schmidt

Department of Physics, Montana State University, Bozeman, MT 59717, USA

A B S T R A C T

$Ba(Ce_{0.8}Y_{0.2})O_{3-\delta}$ anode-supported proton conductive solid oxide fuel cells were fabricated and tested. By changing the H_2 partial pressure at the anode side, the effect of anodic concentration polarization on open-circuit voltage of the cell was observed. Saturation current densities under concentration polarization were obtained from different anode thickness cells and were used for tortuosity calculation. The calculation is based on the dusty-gas model which includes Knudsen diffusion and Stefan–Maxwell equation terms. The tortuosity value for our supporting anode is 1.55 ± 0.1 which is in a physically reasonable range for modern porous anode materials. The tortuosity that we found is independent of the cell testing temperature and anode thickness, which is consistent with the fact that tortuosity is a geometric factor of the anode structure. The derived equation also can be used for predicting the effect of varying the anode thickness, porosity and pore size. Also, the concentration of the gases as a function of position across the anode is determined.

1. Introduction

Strong efforts of modern solid oxide fuel cell (SOFCs) designs are in progress to extend the operating temperature down to the 600–800 °C range. The low operating temperature would increase the benefit of using low cost interconnect material, such as stainless steel, and also reduce problems associated with thermal expansion, atomic migration and corrosion. Accordingly, the electrolyte is made as thin as possible to reduce ohmic loss from transferring ions through electrolyte. The electrolyte thickness is usually down to 20 μm range and requires that an electrode layer, usually the anode, must be made thick enough to mechanically support the cell.

With a thicker anode, gas concentrations at the anode–electrolyte interface need to be calculated carefully because they strongly affect the terminal voltage V as a function of electrolyte current density i, especially in the high current density range. A key parameter in determining the pressure gradient is the tortuosity τ. The definition of 'tortuosity' is

$$\text{tortuosity} = \frac{\text{typical diffusion path between two points through the pores}}{\text{straight distance betwee the same two points}}$$

and sometime is confused with 'tortuosity factor' which is defined as

$$\text{tortuosity factor} = (\text{tortuosity})^2$$

Measurement of its value is needed for determining the quality of the anode pore configuration and necessary for any $V(i)$ modeling. Many modern SOFC models do not adequately calculate the value of τ and invoke anode tortuosities in the range as high as 10–17 [1,2]. Such high tortuosities do not seem physically reasonable when the porosity is usually higher than 30% of the supporting anode.

The impact of such high tortuosity (10–17) is to produce concentration polarization easily when running the cell. With this misleading analysis, one might think sacrificing the structural integrity to decreasing the anode thickness or increasing its porosity is advantageous. However, recent studies of SOFC supporting anodes using focused ion beam scanning electron microscopy (FIB-SEM), X-ray computed tomography and gas counter-diffusion provide evidence that the tortuosity for typical supporting anodes is 1.33–4.0 [3–5]. The present work provides another way for finding tortuosity of the supporting anode for proton conductive solid oxide fuel cells (H-SOFCs) by finding saturation current density under concentration polarization of H-SOFC and using the dusty-gas model. Tortuosity calculations from our tested cells indicate that high tortuosity values may not be correct. The results also provide more accurate information for SOFC design and $V(i)$ modeling.

* Corresponding author. Tel.: +1 406 994 6150; fax: +1 406 994 4452.
E-mail address: tsai@physics.montana.edu (C.-L. Tsai).

0378-7753/$ – see front matter
doi:10.1016/j.jpowsour.2010.08.005

Nomenclature

a	anode forward attempt current density ($A\,cm^{-2}$)
a_0	open-circuit value of a ($A\,cm^{-2}$)
a_{01}	open-circuit value of a when $p_{H_2} = 1$ atm ($A\,cm^{-2}$)
$a_{ele}^3/3$	unit volume of oxygen ion in unit lattice of electrolyte material (cm^3)
D_{Ki}	Knudsen diffusion coefficient for component i ($cm^2\,s^{-1}$)
D_{ij}	binary diffusion coefficient ($cm^2\,s^{-1}$)
D_{ij1}	binary diffusion coefficient when total pressure $P_1 = 1$ atm ($cm^2\,s^{-1}$)
f_a	fraction of oxygen sites at the anode–electrolyte interface
i	SOFC current density ($A\,cm^{-2}$)
i_{as}	saturation current density under anodic concentration polarization ($A\,cm^{-2}$)
J_i	molecular flow densities of gas i ($molec\,s^{-1}$)
$j_{i,m}$	metered inflow rates of gas i ($molec\,s^{-1}$)
$j_{i,net}$	net inflows into the plenum of gas i ($molec\,s^{-1}$)
k	Boltzmann's constant, 1.38×10^{-23} ($J\,K^{-1}$)
M_i	molar mass of the diffusing gas i ($g\,mol^{-1}$)
m_i	molecule mass of component i ($g\,molec^{-1}$)
n_i	concentration of component i ($molec\,cm^{-3}$)
n_1	total gas concentration in the plenum when $P = 1$ atm ($molec\,cm^{-3}$)
$n_{i,p}$	concentration of component i in the plenum ($molec\,cm^{-3}$)
$n_{H_2,as}$	H_2 concentration at the anode–electrolyte interface under saturation current density ($molec\,cm^{-3}$)
$n_{i,p,as}$	concentration of gas i in the plenum at the outer anode surface under saturation current density ($molec\,cm^{-3}$)
$n_{H,ele}$	proton concentration in the electrolyte material (cm^{-3})
P	total pressure
q	charge transfer per reaction, 3.2×10^{-19} (C)
$\bar{r}$	mean pore radius (m)
T	absolute temperature (K)
U_a	enthalpy released when the reaction at anode–electrolyte interface occurs ($J\,kgel^{-1}$)
V	SOFC terminal voltage (V)
V_a	potential difference across the anode–electrolyte interface (V)
v_{ele}	probability of oxygen ion vacancy in electrolyte material
w	anode thickness (cm)

Greek letters

σ_{ij}	average collision diameter of molecules i and j (Å)
τ	tortuosity
ϕ	porosity of supporting anode
Ω	dimensionless collision integral

2. Experimental procedures

The $Ba(Ce_{0.8}Y_{0.2})O_{3-\delta}$ powder was prepared from solid state reaction. Stoichiometric amounts of barium carbonate ($BaCO_3$, 99.8%), cerium oxide (CeO_2, 99.97%), and yttrium oxide (Y_2O_3, 99.99%) were mixed by an agate auto-grinding machine for two hours. Then, the powder was calcined at 1100 °C for 15 h to form the perovskite phase. An X-ray diffraction (Scintag, XGEN-400) with Cu Kα (λ = 1.5418 Å) was used for checking the formation of $Ba(Ce_{0.8}Y_{0.2})O_{3-\delta}$. The auto-grinding and calcining processes were repeated until a single phase of the material was confirmed by the X-ray diffraction.

To prepare the supporting anodes, the $Ba(Ce_{0.8}Y_{0.2})O_{3-\delta}$ powder was weighed and mixed with NiO at volume ratio 1 to 2. In addition to ceramic powders, 8 wt% cornstarch of the total solid load was added to the powder and auto-grinded for 2 h to serve as pore former. The powders were uniaxial die-pressed with a 3/4″ die to form green pellets to serve as the supporting anode. Then, the anode interlayer, with a 1:1 volume ratio of $Ba(Ce_{0.8}Y_{0.2})O_{3-\delta}$ to NiO, and the electrolyte were paint brushed on the supporting anode using the inks prepared by mixing the solid powders with alpha terpinol, ethylcellulose, oleic acid and xylene using a three roll mill. After the drying of electrolyte ink, the pellets were re-pressed by the uniaxial die press and sintered in air at a temperature of 1400 °C for 5 h to form a well-bonded electrolyte–anode structure. Cathode material, $La_{0.8}Sr_{0.2}MnO_3$ (LSM), was then applied on the sintered pellets by paint brush and fired to 1000 °C in air for 2 h to form a good bond between cathode and electrolyte.

A home-made seal-less testing system made from Inconel 600 was used for the measurements, Fig. 1. Silver mesh and nickel foam were used as cathode and anode current collectors, respectively. The total input gas flow rates on each side were controlled by MKS mass flow controllers at 200 ml min^{-1} in all experiments. The water vapor concentration in fuel gas was about 3% by flowing the fuel gas through a water bubbler at room temperature. Measurements were carried out at 700 and 800 °C in ambient pressure. All cells were reduced in situ at high temperature in a 60% H_2 + 40% N_2 mixture for more than an hour prior to the measurements. All performance of the cells was measured using various fuel gas mixtures, i.e. at various partial pressures of H_2/N_2 ratio in fuel gas while the total flow rate of the gas was kept constant at 200 ml min^{-1}. The current densities were calculated based on the cathode area.

Porosity of the supporting anode was measured using Archimedes' method. Each of the tested cells, after reducing, was broken into two pieces. One of the pieces was polished to erase the cathode and electrolyte layers and cleaned with an ultrasonic bath in ethanol. The sample was then kept in a dry oven at 95 °C for more than 2 h to evaporate the ethanol. Dry weight, W_{dry}, wet weight, W_{wet}, and weight saturated with ethanol, W_{sat}, were measured using a high accuracy balance. Prior to measuring W_{wet} in ethanol, the sample was immersed in ethanol and kept in vacuum for 10 min to remove possible air in the pores. The W_{sat} was measured in air soon after the surface of the sample was shaken dry. 'Porosity' was calculated using the equation

$$\text{Porosity}\ (\%) = \frac{W_{sat} - W_{dry}}{W_{sat} - W_{wet}} \times 100\% \quad (1)$$

The other part of the cell was hardened in an epoxy and polished. Field Emission Scanning Electron Microscopy (SUPRA™ 55 Versatile High Performance FE-SEM, Zeiss) was used to examine the microstructure of the cell. The mean pore radius of the cell was determined by quantitative measurements of the pore size on SEM images.

3. Dusty-gas model for gas flow in anode-supported H-SOFC pores

The multi-gas diffusion process in pore structure is generally described by the dusty-gas model, which includes the Stefan–Maxwell equation and Knudsen terms. The equation in

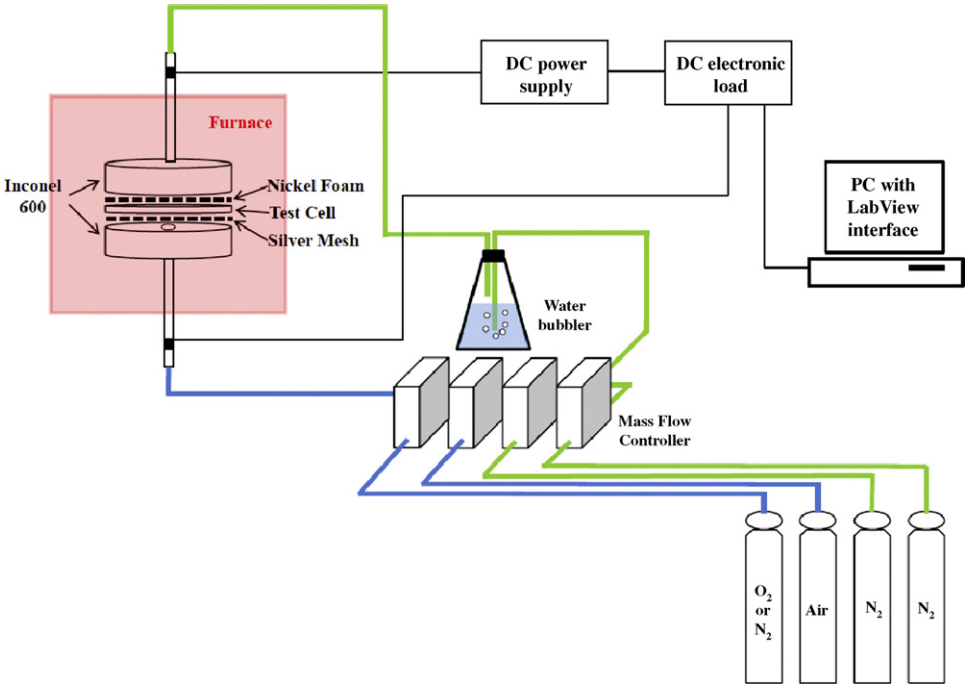

Fig. 1. Schematic of fuel cell test system.

molecular units is [6]

$$\frac{J_i}{D_{Ki}} + \frac{(J_i n_j - J_j n_i)kT}{D_{ij1}P_1} = -\frac{\partial n_i}{\partial x} \tag{2}$$

where J_i and J_j are molecular flow densities of components i and j (molec s^{-1}), respectively, D_{Ki} is the Knudsen diffusion coefficient for component i, D_{ij1} is the binary diffusion coefficient at $P_1 = 1$ atm, and the nkT-type terms in the numerator divided by P_1 convert D_{ij1} to D_{ij}, the binary diffusion coefficient, at the actual total pressure at any position x along the anode pore, n_i and n_j are the concentration of components i and j, k is Boltzmann's constant, 1.38×10^{-23} J K^{-1}, and T is the absolute temperature. It is important to clarify that x in Eq. (2) is the coordinate along a typical gas diffusion path, not across the anode. Therefore, the total diffusion path length is τw, the product of the tortuosity and the anode thickness.

The Knudsen diffusion coefficient considers the collisions between gas molecules and the wall. The equation for the Knudsen diffusion coefficient from the kinetic theory of gases is

$$D_{Ki} = \frac{2}{3}\left(\frac{8kT}{\pi M_i}\right)^{1/2}\bar{r} \tag{3}$$

where $\bar{r}$ is the mean pore radius and M_i is the molar mass of the diffusing gas. The calculated Knudsen diffusion coefficients for H_2, N_2 and H_2O at 700 and 800 °C are listed in Table 1(a).

Table 1
Calculated (a) Knudsen and (b) binary diffusion coefficients for various gases at 700 and 800 °C with $\bar{r} = 1.41$ μm.

(a)			
D_{Ki} (cm^2/s)	H_2	N_2	H_2O
800 °C	31.68	8.47	10.56
700 °C	30.17	8.06	10.06
(b)			
D_{ij1} (cm^2/s)	H_2–N_2	H_2–H_2O	N_2–H_2O
700 °C	5.35	6.65	1.87
800 °C	6.10	7.70	2.21

The binary diffusion coefficient, D_{ij}, is calculated using the Chapman–Enskog equation from Cussler [7]

$$D_{ij} = \frac{1.86 \times 10^{-3} T^{2/3}\left(\frac{1}{M_i} + \frac{1}{M_j}\right)^{1/2}}{P\Omega\sigma_{ij}^2} \tag{4}$$

where Ω is a dimensionless collision integral, based on the Lennard–Jones potential, σ_{ij} is the average collision diameter of molecules i and j (in Å), M_i and M_j are molar masses of diffusion gases i and j, respectively, and P the total pressure (in atm). Using Table 2.2 and 2.3 in Cussler for Ω and σ_{ij} and total pressure $P = 1$ atm, the calculated D_{ij1} for various gases at temperature 700 and 800 °C are listed in Table 1(b).

The experiments were performed with flow of H_2/N_2 gas mixtures to the anode of $Ba(Ce_{0.8}Y_{0.2})O_{3-\delta}$ anode-supported SOFCs. The H_2/N_2 gas mixture picked up H_2O (steam) through a water bubbler so that it is a ternary system, or a binary system when 100% H_2 was used. The flow density of H_2 is $J_{H_2} = i\tau^2/\phi q$, where i is the current density (A cm^{-2} = C cm^{-2} s^{-1}) in the solid electrolyte and q is the charge (3.2×10^{-19} C molec^{-1}) carried per H_2 molecule annihilated in the reaction at the anode/electrolyte interface.

The τ^2/ϕ factor is an enhancement factor by which the flow density J_{H_2} is enhanced compared to its value if the anode were completely porous (i.e. $\phi = \tau = 1$). To derive this result, consider a simple model for which the anode has pores of circular cross-section which are tilted at an angle θ away from the normal to the anode–electrolyte interface. The tortuosity τ (actual path length divided by anode thickness) is $1/\cos\theta$. The flow velocity component perpendicular to the interface is a fraction $\cos\theta$ of the velocity in the pore, so this contributes a factor τ to the enhancement factor. A plane parallel to that interface has pore area fraction ϕ compared to the total area, thereby contributing a factor $1/\phi$ to the enhancement factor. The pore area intercepted by this plane has elliptical shape, but the flow is perpendicular to the pore's circular cross-section which is smaller by a factor $\cos\theta$, so this contributes another factor τ to the enhancement factor. In earlier work [6] we overlooked this final factor and incorrectly used τ/ϕ as the enhancement factor.

We know that there is no N_2 and H_2O flow in the supporting anode, i.e. $J_{N_2} = 0$ and $J_{H_2O} = 0$. Eq. (2) can then be written as

$$\frac{\partial n_{H_2}}{\partial x} = -\left(\frac{i\tau^2}{\phi q}\right)\left(\frac{1}{D_{K,H_2}} + \frac{n_{N_2}kT}{D_{H_2,N_2,1}P_1} + \frac{n_{H_2}kT}{D_{H_2,H_2O,1}P_1}\right) \tag{5a}$$

$$\frac{\partial n_{N_2}}{\partial x} = \frac{i\tau^2}{\phi q}\frac{n_{N_2}kT}{D_{N_2,H_2,1}P_1} \quad \text{and} \tag{5b}$$

$$\frac{\partial n_{H_2O}}{\partial x} = \frac{i\tau^2}{\phi q}\frac{n_{H_2O}kT}{D_{H_2,H_2O,1}P_1} \tag{5c}$$

In reviewing mass transport modeling literature, none of the paper apply this enhancement factor in their calculation [8–11]. Nevertheless, an effective diffusion coefficient was used for the calculations without further explanation, which is in general defined as

$$D_i^{eff} = \frac{\phi}{\tau}D_i \tag{6}$$

where D_i^{eff} and D_i are effective and general diffusion coefficient of species i, respectively. However, after carefully reviewing the FIB-SEM and XCT articles [3,5], and considering discussion of diffusion-based tortuosity analysis by Moldrup et al. [12] and of confusion between tortuosity and tortuosity factor by Epstein [13], it appears that the "tortuosity" in these articles and in Eq. (6) should be "tortuosity factor" which is τ^2. Then our enhancement factor τ^2/ϕ agrees with the ones used in Refs. [3,5] and [8–11].

Adding Eqs. (5a)–(5c) yields the equation for total concentration n and its solution

$$\frac{\partial n}{\partial x} = -\left(\frac{i\tau^2}{\phi q}\frac{1}{D_{K,H_2}}\right) \quad \text{and} \quad n = n_{total,p} - \frac{i\tau^2 x}{\phi q D_{K,H_2}} \equiv n_{total,p} - c_{H_2}\tau^3 \tag{8}$$

where $n_{total,p}$ is the total gas concentration in the plenum and $x = y\tau$ is used in the equation, where y is position on a straight line going across the anode. From the ideal gas law, $P = nkT$, we see that the total pressure P decreases linearly with x from the anode–plenum interface to the solid electrolyte.

We can solve Eq. (5a), (5b) and (5c) for n_{H_2}, n_{N_2} and n_{H_2O}

$$n_{N_2} = n_{N_2,p}\exp\left(\frac{i\tau^2 x}{n_1\phi q D_{H_2,N_2,1}}\right) \equiv n_{N_2,p}\exp(c_{N_2}\tau^3) \tag{8a}$$

$$n_{H_2O} = n_{H_2O,p}\exp\left(\frac{i\tau^2 x}{n_1\phi q D_{H_2,H_2O,1}}\right) \equiv n_{H_2,p}\exp(c_{H_2O}\tau^3) \quad \text{and} \tag{8b}$$

$$n_{H_2} = n_{H_2,p} - c_{H_2}\tau^3 - n_{N_2,p}(\exp(c_{N_2}\tau^3) - 1) - n_{H_2O,p}(\exp(c_{H_2O}\tau^3) - 1) \tag{8c}$$

where $n_{N_2,p}$, $n_{H_2O,p}$ and $n_{H_2,p}$ are concentrations for N_2, H_2O and H_2 in the plenum, respectively, n_1 is the total gas concentration in the plenum when $P = 1\,\text{atm} = 1.015 \times 10^5\,\text{N m}^{-2}$, $n_1 = P_1/kT$ and $n_1 = 7.559 \times 10^{18}\,\text{cm}^{-3}$ for $T = 973\,\text{K}$ and $n_1 = 6.855 \times 10^{18}\,\text{cm}^{-3}$ for $T = 1073\,\text{K}$. We see that n_{N_2} and n_{H_2O} increase exponentially along the pore from plenum to electrolyte.

If the cell current density is saturated by concentration polarization at the anode, designated as i_{as}, then i become i_{as} in the "constants" c_{H_2}, c_{N_2} and c_{H_2O}, which are really linear functions of position x/τ across the anode. For $x/\tau = w$ (the anode thickness) at the anode–electrolyte interface, they really become constants and are designated as $c_{H_2,as}$, $c_{N_2,as}$ and $c_{H_2O,as}$ for the saturated condition.

To find n_{H_2} at the anode–electrolyte interface, we use results from our analysis of H-SOFC voltage V as a function of current density i. The analysis of the I–V curve for H-SOFC is based on the concept of exchange current density, i_0. The exchange current density is defined for open-circuit operation in which the equal and opposite current densities in the system result from the equal forward and reverse reaction rates at the interface of anode–electrolyte, $H_2 \leftrightarrow 2H^+ + 2e^-$, cathode–electrolyte, $2H^+ + O^{2-} \leftrightarrow H_2O$, and cathode-pore, $1/2O_2 + 2e^- \leftrightarrow O^{2-}$. In our model, we propose a two-step cathode reaction mechanism instead of a one-step mechanism. For a one-step cathode reaction, $4H^+ + O_2 + 4e^- \leftrightarrow 2H_2O$, an O_2 molecule is required to react with four protons and four electrons at a cathode TPB site to form $2H_2O$ molecules. However, the concentration of protons in the electrolyte is low (<20%), which makes the probability of four protons simultaneously being within reaction distance is too low to provide the dominant reaction mechanism. Accordingly, there are three exchange current densities, one from the reactions at the anode–electrolyte interface, another from the reactions at the cathode–electrolyte interface and the third from the reactions from the cathode–pore interface.

For closed-circuit operation, we continue to use the concept of forward and reverse reactions and their corresponding current densities. The net current density across the cell comes from the difference between the forward and reverse current densities, each of which is described as the product of an attempt current density and a reaction success probability.

In our model, we treat all the reactions at interfaces as collision events which can be described by classical (Boltzmann) statistics. The forward current density at the anode–electrolyte interface can be described as

$$i_{af} = ae^{\alpha}/2\cosh\alpha, \quad \text{and} \quad \alpha \equiv (U_a - qV_a)/2kT$$

Here a is forward attempt current density and $e^{\alpha}/2\cosh\alpha$ is reaction success probability for the reaction, $H_2 \rightarrow 2H^+ + 2e^-$, at anode–electrolyte interface. U_a is the enthalpy released when the reaction occurs, q is the charge transfer per reaction which is $3.2 \times 10^{-19}\,\text{C}$, and V_a is the potential difference across the anode–electrolyte interface. Thus, $(U_a - qV_a)$ is the net energy required for the reaction to occur. The expression for a is

$$a \equiv \frac{1}{2}n_{H_2}\left(\frac{kT}{m_{H_2}}\right)^{1/2} f_a q(1 - \nu_{ele})(1 - a_{ele}^3 n_{H,ele}/3)^2, \tag{9}$$

where m_{H_2} is the H_2 molecule mass, and $(kT/m_{H_2})^{1/2}$ is the H_2 molecule average velocity component (through the anode pore) directed toward the triple phase boundary (TPB). $(1 - \nu_{ele})(1 - a_{ele}^3 n_{H,ele}/3)^2$ is the probability that an O^{2-} ion without a proton attached to it at the anode TPB so that the H_2 dissociation reaction can occur in which ν_{ele} is the probability of oxygen ion vacancy in electrolyte material, $a_{ele}^3/3$ is the unit volume of oxygen ion in unit lattice of electrolyte material and $n_{H,ele}$ is proton concentration in the electrolyte, and f_a is the fraction of oxygen sites from electrolyte that sit on the TPB and are available for the reaction at the anode–electrolyte interface. The detailed derivation and discussion of our $V(i)$ model will be published elsewhere.

By setting $n_{H_2} = n_{H_2,as}$ under the anode saturation condition, Eq. (8c) can be rewritten as

$$n_{H_2,p,} - c_{H_2,as}\tau^3 - n_{N_2,p,as}(\exp(c_{N_2,as}\tau^3) - 1) - n_{H_2O,p,as}(\exp(c_{H_2O,as}\tau^3) - 1) - n_{H_2,as} = 0 \tag{10}$$

All constants in Eq. (10) are positive and can be solved numerically for τ.

The constants in Eq. (10) have been defined except for the boundary conditions $n_{H_2,p,as}$, $n_{N_2,p,as}$ and $n_{H_2O,p,as}$ for gas concentrations in the plenum at the outer anode surface and $n_{H_2,as}$ for the

H_2 concentration at the anode–electrolyte interface. To find $n_{H_2,p,as}$ we consider the total flow in and out of the anode plenum. For all the experiments, the total gas inflow rate before going through the water bubbler is 200 ml min^{-1}. The total metered inflow rate of 200 ml min^{-1} at temperature 21 °C and at Bozeman, Montana atmosphere (4900 ft. above sea level, $P_{Bozeman} = 8.534 \times 10^4$ N m^{-2}) is, from the ideal gas law,

$$P_{Bozeman}\frac{dV_{in}}{dt} = kT_{in}\frac{dN_{in}}{dt}, \text{ so } \frac{dN_{in}}{dt} \equiv j_1 = 7.012 \times 10^{19} \text{ molec s}^{-1} \quad (11)$$

The metered inflow H_2 is found by multiplying the total metered inflow rate by the partial pressure fraction, and N_2 is the balance of the total inflow. Because H_2O is obtained by flowing the inflow gas through a water bubbler, the flow rate of H_2O is the inflow rate multiplied by saturated water partial pressure at room temperature (3%). For example, a 20% H_2 input gas flow has metered flow rates: $j_{H_2,m} = p_{H_2} j_1 = 1.404 \times 10^{19}$ molec s^{-1}, $j_{N_2,m} = p_{N_2} j_1 = 5.618 \times 10^{19}$ molec s^{-1} and $j_{H_2O,m} = p_{H_2O,sat} j_1 = 2.107 \times 10^{18}$ molec s^{-1}.

To find the net flow of each gas into the plenum, we must consider the fuel gas, H_2, outflow into the anode. The inflow rate of H_2 into anode is $j_{H_2} = -iS/q$, where S is the active area and $q = 3.2 \times 10^{-19}$ C. When the cell is running at saturation current, the inflow rate into the anode is designated as $j_{H_2,as}$. To summarize the analysis for net inflows into the plenum,

$$j_{H_2,net} = p_{H_2} j_1 - \frac{iS}{q}, \quad j_{N_2,net} = p_N j_1, \quad j_{H_2O,net} = p_{H_2O,sat} j_1 \text{ and } j_{total,net} = j_{H_2,net} + j_{N_2,net} + j_{H_2O,net} \quad (12)$$

Our test system is open to space and we assume that the gases in the plenum are well mixed and have the same mole fraction everywhere. Accordingly, in the plenum the gas concentrations under anode saturation conditions are

$$n_{total,p} = \frac{P_{Bozeman}}{kT}, \quad n_{H_2,p,as} = \left(\frac{j_{H_2,net,as}}{j_{total,net,as}}\right) n_{total,p}$$
$$n_{N_2,p,as} = \left(\frac{j_{N_2,net}}{j_{total,net,as}}\right) n_{total,p} \text{ and} \quad (13)$$
$$n_{H_2O,p,as} = \left(\frac{j_{H_2O,net}}{j_{total,net,as}}\right) n_{total,p}$$

The remaining parameter to determine is $n_{H_2,as}$, the H_2 concentration at the anode–electrolyte interface under the anode saturation condition. From Eq. (9), n_{H_2} remains proportional to a as i changes, because we assume the other parameters are independent of i. For open-circuit ($i = 0$) conditions, n_{H_2} at the interface equals $n_{H_2,0} = p_{H_2} n_{total,p}$. This known value for open-circuit n_{H_2} inserted into Eq. (9) provides a known value $a_0 = p_{H_2} a_{01}$ for the open-circuit value of a, where a_{01} is the open-circuit value for $p_{H_2} = 1$ and is 510.60 and 486.22 A cm^{-2} for 700 and 800 °C, respectively. For the anode saturation condition, $a = i_{as}$, and because n_{H_2} is proportional to a, we have

$$n_{H_2,as} = \frac{n_{H_2,0} a_{as}}{a_0} = \frac{p_{H_2} n_{total,p} i_{as}}{p_{H_2} a_{01}} = \frac{n_{total,p} i_{as}}{a_{01}} \quad (14)$$

Inserting the $n_{H_2,as}$ value and the $n_{H_2,p,as}$ value into Eq. (10) yields the following equation for τ^3 in terms of known parameters

$$\left(\frac{j_{H_2,net,as}}{j_{total,net,as}}\right) n_{total,p} - c_{H_2,as}\tau^3 - n_{N_2,p,as}(\exp(c_{N_2,as}\tau^3) - 1)$$
$$- n_{H_2O,p,as}(\exp(c_{H_2O,as}\tau^3) - 1) - \frac{n_{total,p} i_{as}}{a_{01}} = 0 \quad (15)$$

4. Results and discussion

For the purpose of tortuosity investigation, a series of different thickness anode-supported $Ba(Ce_{0.8}Y_{0.2})O_{3-\delta}$ H-SOFCs, from 1.85 to 1 mm, were made and tested. Fig. 2 shows the cross-section microstructure of one of the tested $Ba(Ce_{0.8}Y_{0.2})O_{3-\delta}$ anode-supported cells from SEM. The dense electrolyte is ~20 μm in thickness and adheres to a ~35 μm anode interlayer very well. The thickness of porous cathode is ~45 μm. The mean pore radius of the supporting anodes estimated quantitatively from SEM micrographs was ~1.41 μm. The porosity of the supporting anode was ~34%, which was measured using Archimedes' method described in the experimental procedures. This porosity only refers to open pores of the supporting anode since closed pores do not provide channels for gas diffusion.

The electrochemical performances of a $Ba(Ce_{0.8}Y_{0.2})O_{3-\delta}$ anode-supported H-SOFC with a 1.5 mm-thick anode are shown in Fig. 3. The tests were done at temperature 700 °C, Fig. 3(a), and 800 °C, Fig. 3(b), under different H_2 partial pressures while air was used as oxidant at the cathode. The near linear I–V curves of the cell performance at high H_2 partial pressures, >40% H_2, indicate the domination of ohmic polarization of the cell outputs. For low H_2 partial pressures, less than 30%, the convex I–V curvatures indicates the activation and ohmic polarization loss of the cell are small compared to the concentration polarization, especially when the cell was running at high current density. The concentration polarization effect from changing H_2 partial pressures also shows up with the decreasing of open-circuit voltage when H_2 partial pressure decreases, Fig. 4. When comparing the open-circuit voltage (OCV) of H_2/air gas inputs, our OCV is lower than the theoretical value, by about 0.1 V at 700 °C and 0.122 V at 800 °C. This is because of the redox reaction of Ce^{3+}/Ce^{4+} in $Ba(Ce_{0.8}Y_{0.2})O_{3-\delta}$ under reducing atmosphere, which increases the electronic conductivity of the electrolyte and results in lower OCV. The electronic conductivity of $Ba(Ce_{0.8}Y_{0.2})O_{3-\delta}$ increases with increasing operating temperature, which explains the bigger voltage difference of OCV between the theoretical EMF and measured OCV at 800 °C. Similar results were reported when using lanthanum-doped ceria and zirconium-doped BCY as electrolyte for SOFCs [14–19].

When examining the I–V curves from $Ba(Ce_{0.8}Y_{0.2})O_{3-\delta}$ anode-supported cells, we notice the current density increases rapidly at low voltage, e.g. at voltage lower than 0.05 V for 10% H_2 partial pressure in Figs. 3(b) and Fig. 5(a). The same feature is reproducible and was also seen on the anode thickness of 1.34 and 1.84 mm but not

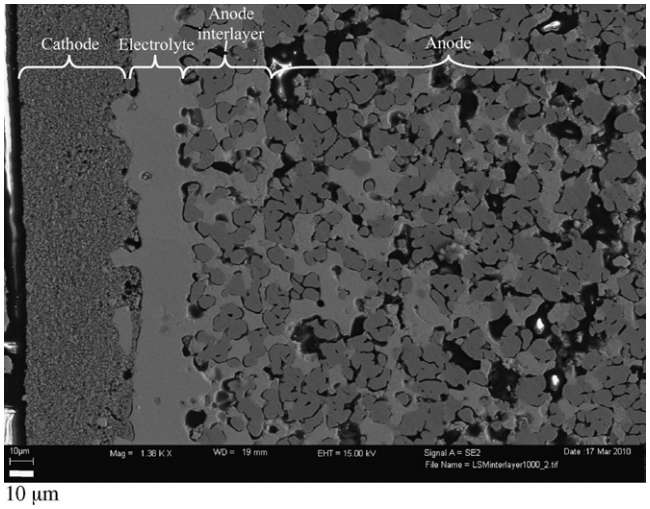

Fig. 2. Microstructure of $Ba(Ce_{0.8}Y_{0.2})O_{3-\delta}$ anode supported H-SOFC from SEM image.

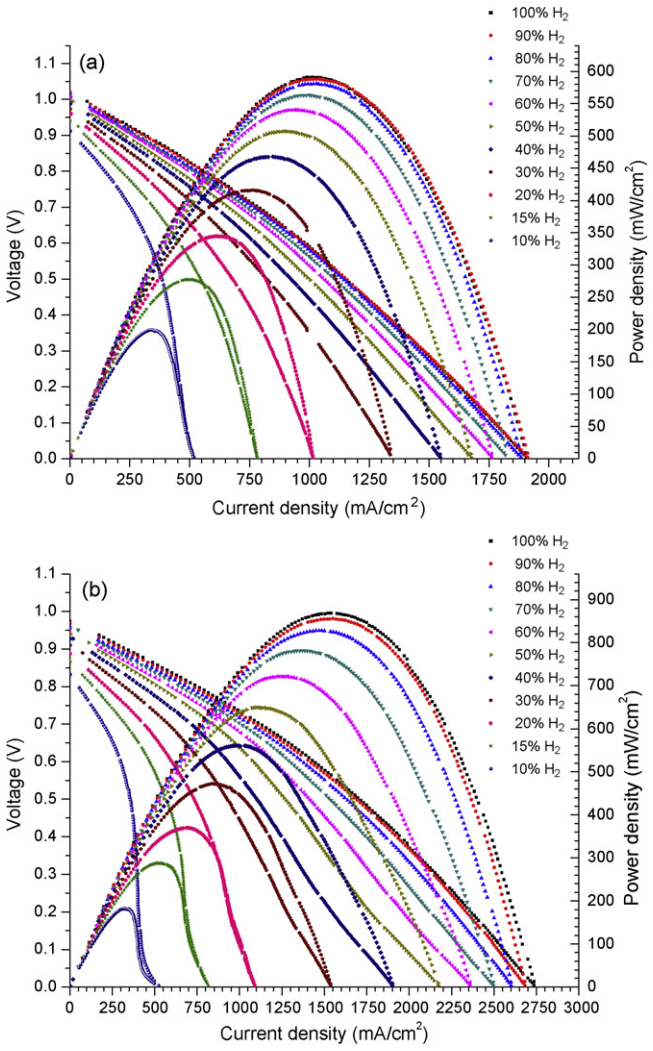

Fig. 3. Hydrogen partial pressure dependent electrochemical performance of $Ba(Ce_{0.8}Y_{0.2})O_{3-\delta}$ anode supported H-SOFC with 1.5 mm anode thickness at (a) 700 °C and (b) 800 °C.

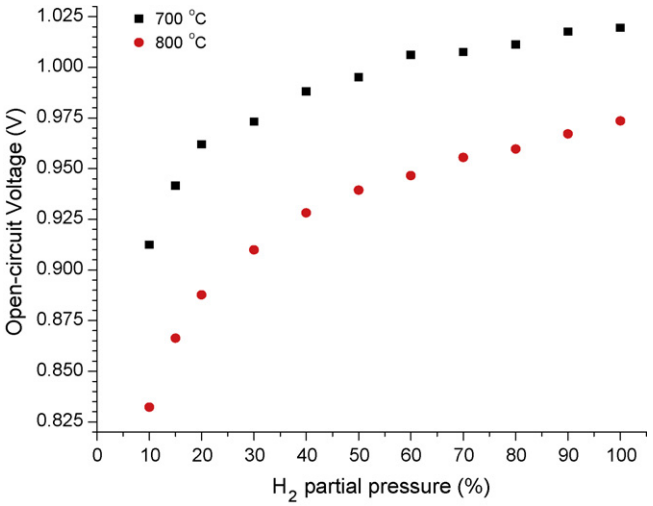

Fig. 4. Open-circuit voltage of $Ba(Ce_{0.8}Y_{0.2})O_{3-\delta}$ anode supported H-SOFC with 1.5 mm anode thickness.

on 1 mm cells. It seems the "tail" gets bigger when the supporting anode gets thicker. The cell with 1.5 mm anode thickness was specifically run with 20% H_2 partial pressure under 0.1 V for more than 13 h at 800 °C before the test system was shut down. Since the cell can be run for a long period, it excludes the possibility that the electrolyte was giving up its oxygen ion for the SOFC reaction, i.e. the electrolyte was not decomposing and cannot provide the cell an extra oxygen source. Conventionally, we expect a straight down *I–V* curve when concentration polarization dominates, using up all of the fuel gas at the anode–electrolyte interface, and giving a saturation current density. This behavior indicates a mechanism faster than gas diffusion dominated supply of fuel gas to the TPB. Our speculation on this mechanism is surface diffusion of protons along Ni surface to the TPB. For H-SOFC, protons diffusing along Ni surface allows them to incorporate into electrolyte at the TPB and provides enough protons for the reaction on the cathode side, i.e. $2H^+ + O^{2-} \leftrightarrow H_2O$. The same mechanism was not seen on our O-SOFC, 8 mol% yttria-stabilized ZrO_2 cells, because two protons must meet an O^{2-} at the TPB at the same time for the reaction to occur on the anode side. However, Williford et al. and Lee et al. point out that surface diffusion of protons along Ni surface occurs only over small distance and lower speed when compared to bulk gas diffusion [4,8]. Therefore, the reason for the "tail" behavior remains unclear.

Due to the fact that *a* was obtained from the modeling of impinging rate of H_2 onto the triple phase boundary (TPB), the amount of n_{H_2} present at the anode–electrolyte interface determines the saturation current density when *V* goes to zero. Therefore, we took the current density as i_{as} when the voltage drops to zero in the *I–V* curve measurements. Values of i_{as} for various hydrogen partial pressures appear in Table 2. Fig. 5 shows the results from our tortuosity calculations and the electrochemical performances of a $Ba(Ce_{0.8}Y_{0.2})O_{3-\delta}$ anode-supported H-SOFC with an anode thickness 1.84 mm. The shown data is for tests at 800 °C under different H_2 partial pressures. The tortuosity results range from 2.94 to 1.50, but are limited to a value around 1.50 when H_2 concentrations are below 20%. As shown in Fig. 5(a), the cell performances did not encounter serious concentration polarization at H_2 partial pressure above 50%. For H_2 partial pressure above 50%, the main loss was

Table 2
List of saturation current densities for different anode thicknesses which were tested under different H_2 partial pressures at (a) 800 °C and (b) 700 °C.

p_{H_2}	i_{as} (A cm^{-2}) Anode 1.84 mm	i_{as} (A cm^{-2}) Anode 1.50 mm	i_{as}(A cm^{-2}) Anode 1.34 mm	i_{as} (A cm^{-2}) Anode 1.00 mm
(a)				
10%	0.506	0.522	0.709	0.854
15%	0.782	0.816	0.955	1.174
20%	1.055	1.091	1.193	1.410
30%	1.489	1.537	1.493	1.686
(b)				
10%	0.543	0.517	0.619	0.757
15%	0.721	0.782	0.802	1.058
20%	0.846	1.015	0.950	1.294
30%	1.005	1.338	1.117	1.590

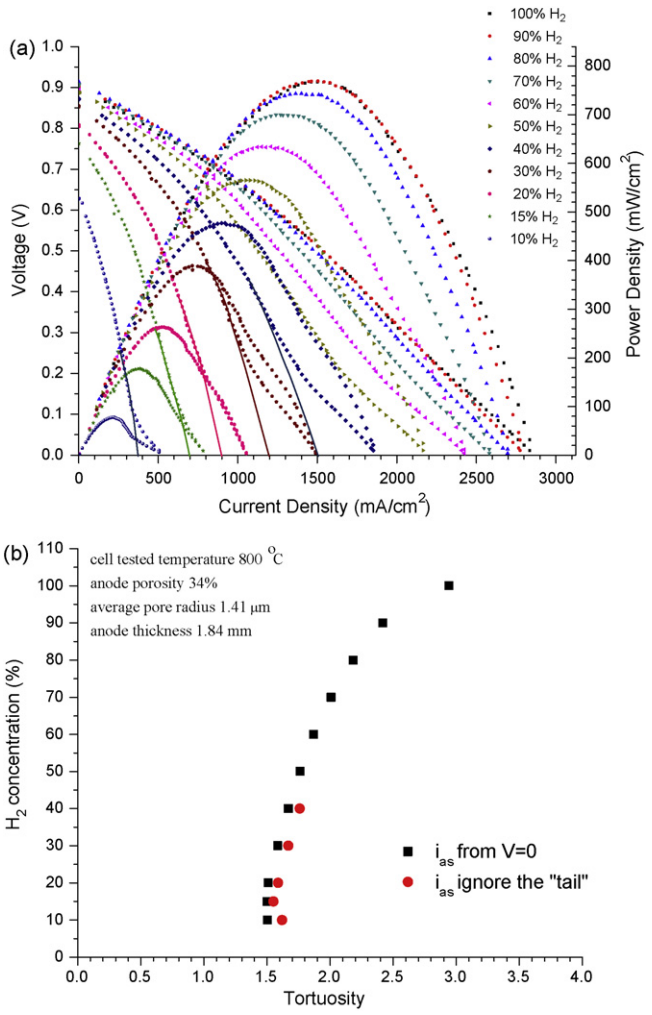

Fig. 5. $Ba(Ce_{0.8}Y_{0.2})O_{3-\delta}$ anode-supported H-SOFC (a) the electrochemical performance at 800 °C under different H_2 partial pressures and (b) calculated tortuosities for its anode.

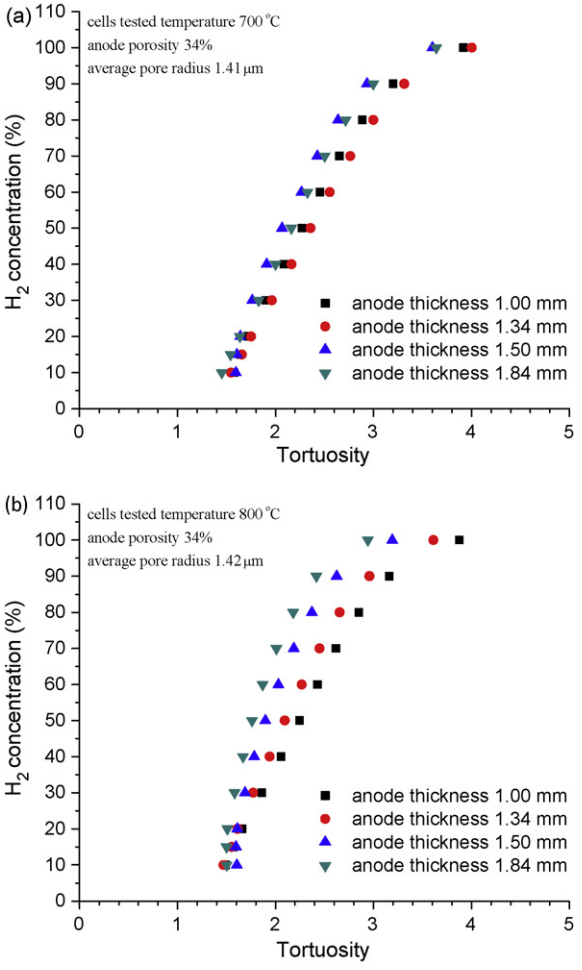

Fig. 6. Calculated tortuosities for different thickness anode cells tested at (a) 800 °C and (b) 700 °C.

from ohmic polarization so that the calculated tortuosity using i_{as} at voltage drop to zero should not be considered. Note that when concentration polarization is severe, the tortuosity values approach the same value. Therefore, the tortuosity calculated from lowest H_2 concentrations should be a more accurate number. Fig. 5(b) also shows the calculated tortuosity for H_2 partial pressure under 40% when the "tail" effect is ignored, using the intersect value between solid lines and current density axis in Fig. 5(a). The tortuosity is then increasing from ~1.50 to ~1.60 at low H_2 concentration.

$Ba(Ce_{0.8}Y_{0.2})O_{3-\delta}$ anode-supported cells with different anode thickness, but the same porosity and pore radius, were tested and the tortuosities of their anodes were also calculated. The results are shown in Fig. 6. The tortuosities obtained from 10% H_2 concentration all fall into the same range, 1.55 ± 0.1, and are thickness independent, as they should be, for the tests both at 800 and 700 °C. Compared to 700 °C, the tortuosity values approach their final value at higher H_2 concentration when cells were tested at 800 °C. This is because of the higher fuel utilization of cells at 800 °C that makes the cells encounter concentration polarization at higher H_2 partial pressure.

We compare the result presented here, 1.55 ± 0.1 with our previous results from analyzing Jiang–Virkar's experiment which was 2.3 ± 0.6 [6,14]. If we take into account that the enhancement factor should have been τ^2/ϕ, then the new number in Ref. [6] is 1.74 ± 0.3. The tortuosity value presented here is a little smaller than the previous average value but within the error. This results from our bigger pore radius, 1.41 μm, when compared to Jiang–Virkar's 0.5 μm pore radius, even though our porosity is lower, 34%, compared to their 54% porosity. When looking at Jiang–Virkar's 20%H_2–80%N_2-H_2O ternary system, its saturation current i_{as} is 0.89 A cm^{-2}. The test in Fig. 4 with 20% H_2 partial pressure delivered a saturation current 1.055 A cm^{-2} or 0.877 A cm^{-2} when the "tail" is not considered. For our much lower porosity but delivering similar amount of H_2 fuel from plenum to anode–electrolyte interface, it makes sense that our tortuosity is lower, i.e. the pores are straighter from plenum–anode interface to anode–electrolyte interface. Furthermore, the bigger pore size reduces the collision rate of gas molecules with the wall, thereby reducing the effect from Knudsen diffusion, resulting in lower tortuosity of our supporting anode. This value is also similar to the results which were obtained from FIB-SEM, X-ray computed tomography and gas counter diffusion, $\tau = 1.33$–4.0 [3–5].

Plots of gas concentrations across the anode for six different H_2 partial pressures under anode limiting currents at 700 °C are shown in Fig. 7. The total concentrations only decrease slightly because of the compensation from N_2 concentration increasing. The exponential effects on the gas concentrations appear insignificant. They appear more like linear changes, due to the relatively "thin" supporting anode. To see the exponential effects, it is necessary to have a supporting anode thicker than 1 cm and high H_2 partial pressure.

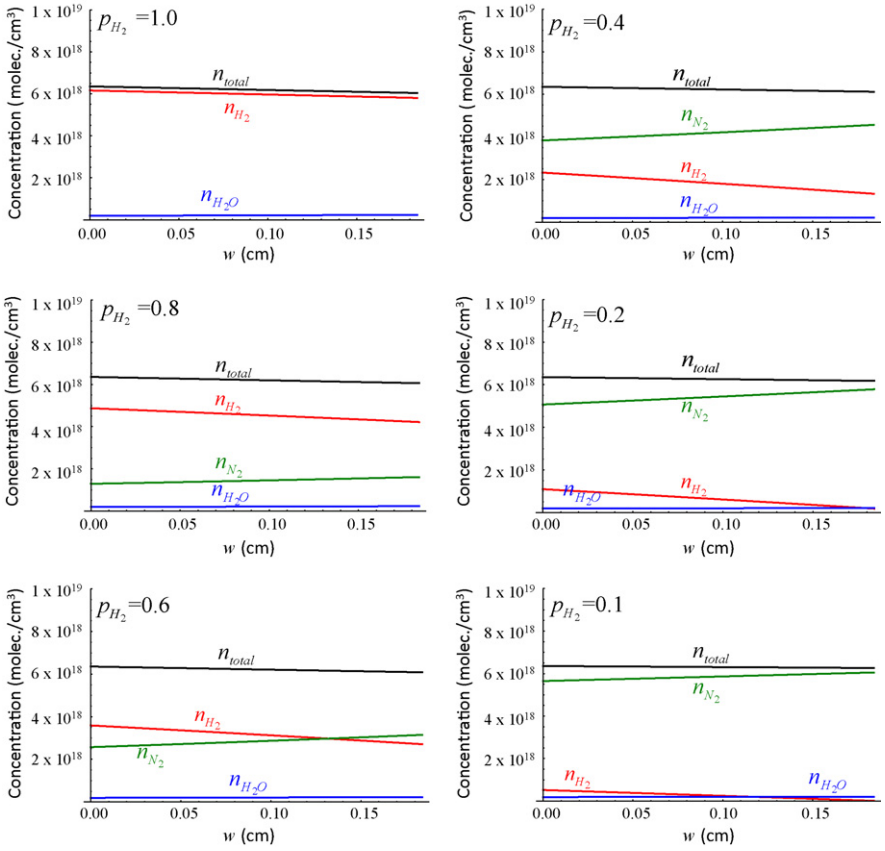

Fig. 7. Plots of gas concentration vs. position in anode for 1.84 mm anode thickness under anode-limiting current conditions at 700 °C.

5. Conclusions

A series of different anode thickness $Ba(Ce_{0.8}Y_{0.2})O_{3-\delta}$ anode-supported H-SOFC were made and tested. By changing H_2 partial pressures, the anodic concentration polarization effect can be observed. For low H_2 partial pressures, saturation current densities under concentration polarization were obtained and used for tortuosity calculation. The result of tortuosity calculation for the supporting anode is 1.55 ± 0.1, which is temperature and thickness independent, as it should be since tortuosity is a geometric factor of the anode structure.

The accurate tests bring down the error between cells to ± 0.1 of the total value. The value of 1.55 ± 0.1 is a little smaller than the average number, which we found previously from analyzing the Jiang–Virkar results, 1.74 ± 0.3. However, the lower porosity and bigger pore size of our supporting anode are consistent with a lower tortuosity to deliver the measured similar amount of H_2 gas from the plenum to the anode–electrolyte interface. Our result is also consistent with the values found by different technologies for modern anode material with typical porosity >30%. Therefore, we can say that our value is in the physically reasonable range. The developed equations also give information for pressure drops across the electrodes and the gas concentrations at the H-SOFC electrode–electrolyte interface which provides the required tools for modeling the voltage–current density expression. Such voltage–current modeling gives information for new SOFC designs and for analyzing performance of existing designs in both fuel cell and electrolysis modes.

Acknowledgements

The authors thank Dr. Stephen W. Sofie for the use of all his facilities. This work was supported by the United States Department of Energy, as a subcontract from Battelle Memorial Institute and Pacific Northwest National Laboratory under Award No. DE-AC06-76RL01830.

References

[1] J.W. Kim, A.V. Virkar, K.Z. Fung, K. Mehta, S.C. Singhal, J. Electrochem. Soc. 146 (1999) 69.
[2] P. Costamagna, K. Honegger, J. Electrochem. Soc. 145 (1998) 3995.
[3] H. Iwai, N. Shikazono, T. Matsui, H. Teshima, M. Kishimoto, R. Kishida, D. Hayashi, K. Matsuzaki, D. Kanno, M. Saito, H. Muroyama, K. Eguchi, N. Kasagi, H. Yoshida, J. Power Sources 195 (2010) 955.
[4] R.E. Williford, L.A. Chick, G.D. Maupin, S.P. Simner, J. Electrochem. Soc. 150 (2003) A1067.
[5] J.R. Izzo Jr., A.S. Joshi, K.N. Grew, W.K.S. Chiu, A. Tkachuk, S.H. Wang, W. Yun, J. Electrochem. Soc. 155 (2008) B504.
[6] V.H. Schmidt, C.-L. Tsai, J. Power Sources 180 (2008) 253.
[7] E.L. Cussler, Diffusion-Mass Transfer in Fluid Systems, Cambridge University Press, Cambridge, MA, 1984.
[8] W.Y. Lee, D. Wee, A.F. Ghoniem, J. Power Sources 186 (2009) 417.
[9] S.C. DeCaluwe, H. Zhu, R.J. Kee, G.S. Jackson, J. Electrochem. Soc. 155 (2008) B538.
[10] W. Lehnert, J. Meusinger, F. Thom, J. Power Sources 87 (2000) 57.
[11] J.R. Izzo Jr., A.A. Peracchio, W.S.K. Chiu, J. Power Sources 176 (2008) 200.
[12] P. Moldrup, T. Olesen, T. Komatsu, P. Schjönning, D.E. Rolston, Soil Sci. Soc. Am. J. 65 (2001) 613.
[13] N. Epstein, Chem. Eng. Sci. 44 (1989) 777.
[14] Y. Jiang, A.V. Virkar, J. Electrochem. Soc. 150 (2003) A942.
[15] Y.-P. Xiong, H. Kishimoto, K. Yamaji, M. Yoshinaga, T. Horita, M.E. Brito, H. Yokokawa, Electrochem. Solid-State Lett. 13 (2010) B21.
[16] S.-H. Park, H.I. Yoo, Phys. Chem. Chem. Phys. 11 (2009) 391.
[17] M. Mogensen, N.M. Sammes, G.A. Tompsett, Solid State Ionics 129 (2000) 63.
[18] H. Ding, X. Xue, X. Liu, G. Meng, J. Power Sources 195 (2010) 775.
[19] L. Yang, Z. Liu, S. Wang, Y. Choi, C. Zuo, M. Liu, J. Power Sources 195 (2010) 471.